Lagrangian irreversibility and energy exchanges in rotating-stratified turbulent flows

S. Gallon,[1] A. Sozza,[1, 2] F. Feraco,[3, 4] R. Marino,[3] and A. Pumir[1, 5]

[1] Univ Lyon, ENS de Lyon, CNRS, Laboratoire de Physique, F-69342 Lyon, France
[2] CNR, Institute of Atmospheric Sciences and Climate, 10133 Torino, Italy
[3] Univ Lyon, CNRS, École Centrale de Lyon, INSA de Lyon, Univ Claude Bernard Lyon 1,
Laboratoire de Mécanique des Fluides et d'Acoustique - UMR 5509, F-69134 Écully, France
[4] Leibniz-Institute of Atmospheric Physics at the Rostock University, 18225 Kühlungsborn, Germany
[5] Max Planck Institute for Dynamics and Self-Organization, 37077 Göttingen, Germany

(Dated: January 25, 2024)

Turbulence in stratified and rotating turbulent flows is characterized by an interplay between waves and eddies, resulting in continuous exchanges between potential and kinetic energy. Here, we study how these processes affect the turbulent energy cascade from large to small scales, which manifests itself by an irreversible evolution of the relative kinetic energy between two tracer particles. We find that when r_0, the separation between particles, is below a characteristic length ℓ_t, potential energy is on average transferred to kinetic energy, reducing time irreversibility, and conversely when $r_0 > \ell_t$. Our study reveals that the scale ℓ_t coincides with the buoyancy length scale L_B over a broad range of configurations until a transitional wave-dominated regime is reached.

The dynamics of rotating and stratified flows, as they occur in the oceans on Earth, in planetary atmospheres and in stars, depend strongly on their rotation rate, natural buoyancy frequency and the ratio between these physical parameters [1, 2]. These flows in nature are in general highly turbulent, with estimated Reynolds numbers of at least Re $> 10^9$ for terrestrial oceans [3], involving a wide range of spatial scales, from the largest flow structures of the order of tens of kilometers (or more in astrophysical frameworks [4]), down to dissipative scales of a few millimeters [3, 5, 6]. Much of our understanding of turbulent flows comes from studying the idealized case of three-dimensional homogeneous isotropic turbulence (HIT), which has been postulated to describe the properties of small-scale motions in the limit of very large Reynolds numbers [7, 8]. In this case, flows are characterized by a flux of kinetic energy from large to small scales, where dissipation occurs at a rate ε_ν. The resulting cascade of energy introduces a fundamental irreversibility of the flow, which has a clear signature on the relative motion of two tracer particles that are initially separated by a distance $r_0 = |\mathbf{r}(0)|$. This property rests on the identity relating the average of the scalar product between their velocity and acceleration differences to the energy dissipation rate $\langle \Delta_{\mathbf{r}_0} \mathbf{u} \cdot \Delta_{\mathbf{r}_0} \mathbf{a} \rangle \approx -2\varepsilon_\nu$, with the Lagrangian acceleration $\mathbf{a} = \mathrm{D}/\mathrm{D}t \, \mathbf{u}$, provided r_0 is in so-called inertial range [9–11]. This relation implies that the relative kinetic energy of pairs of tracers, as well as their separation $\langle (\mathbf{r}(t) - \mathbf{r}_0)^2 \rangle$, are not even functions of time, which allows us to distinguish the time evolutions forwards and backwards in time [12, 13]. We notice that other manifestations of the time-irreversibility have been obtained from Lagrangian turbulence [12, 14].

In geophysical frameworks, turbulent flows are subject to stratification (STRAT) and rotation (ROT), which introduce waves that couple velocity (kinetic energy) and density fluctuations (potential energy) [2, 15]. These waves induce flow instabilities, and lead to the formation of strong vertical drafts, and to turbulence as a result of wave breaking [16–21]. Furthermore, they affect the inter-scale energy transfer leading in some cases to inverse or dual kinetic and/or potential energy cascades [22–24]. Here, we investigate the interaction between kinetic $\mathbf{u}^2/2$ and potential energy $\theta^2/2$ in the flow, their effect on the turbulent cascade and the resulting irreversibility. We revisit the energy budget for such flows using the Boussinesq approximation [2], thereby generalizing the Karman-Howarth-Monin relations to the Lagrangian framework [25]. We establish that the time-symmetry breaking term involves not only the energy dissipation ε_ν, but also an exchange term between potential and kinetic energy.

Numerically, we study the influence of waves and turbulence, keeping fixed the ratio between stratification and rotation in a configuration of oceanographic relevance [26, 27]. In a flow forced by injecting kinetic energy, we observe that at large scales, energy is transferred on average from kinetic to potential energy. We find at smaller scales an inversion of the flux, i.e. from potential to kinetic energy, which is in qualitative agreement with previous numerical observations in spectral space [28–32]. This inversion allows us to identify a characteristic length scale ℓ_t of the flow, which we relate to the typical vertical length scale of stratification layers and therefore the complex interactions of waves and vortices [31, 33, 34].

We perform direct numerical simulations (DNS) of the Boussinesq equations in a rotating frame, with constant solid body rotation rate Ω (and frequency $f = 2\Omega$) and gravity $\mathbf{g}$ anti-aligned in the vertical (z) direction. The fluid is linearly stably stratified, subjected to a mean density profile $\bar{\rho} = \rho_0 - \gamma z$, parameterized by the Brunt-Väisälä frequency $N = (\gamma g/\rho_0)^{1/2}$. The equations of motion for the incompressible velocity field $\mathbf{u}(\mathbf{x}, t) = (u, v, w)$ (e.g. $\boldsymbol{\nabla} \cdot \mathbf{u} = 0$) and the density fluctuation

TABLE I. Parameters of the runs. N Brunt-Väisälä frequency, ν kinematic viscosity, ε_ν kinetic energy dissipation rate (averaged over particle integration time), Fr Froude number, Re Reynolds number, R_{IB} Buoyancy Reynolds number, ℓ_O Ozmidov scale. Runs A0 - A4 where run at a grid resolution of $M = 512$, runs B0 - B4 at $M = 1024$. We set the viscosity to $\nu = 1.5 \cdot 10^{-3}$ for run A0, $\nu = 1 \cdot 10^{-3}$ for runs A0-A4 and $\nu = 2.1 \cdot 10^{-4}$ for runs B0-B1. We integrated the trajectories of $1.5 \cdot 10^6$ particles for runs A0-A4 and $6 \cdot 10^6$ particles for runs B0-B4. All simulations have been run for at least 4.5 eddy turnover times after the insertion of the particles.

Run	A0	A1	A2	A3	A4	B0	B1	B2	B3	B4
N	0	2.95	4.92	7.37	14.7	0	1.18	2.95	7.37	14.7
ε_ν	0.375	0.206	0.156	0.123	0.0237	0.00784	0.00932	0.00715	0.0136	0.0344
Fr	∞	0.169	0.105	0.0777	0.0410	∞	0.155	0.0823	0.0599	0.0356
Re	2380	3140	3270	3620	3820	4790	5510	7300	13300	15800
R_{IB}	∞	23.8	6.47	2.26	0.109	∞	31.9	3.92	1.19	0.755
η	0.00974	0.00834	0.00894	0.00950	0.0143	0.00586	0.00561	0.00600	0.00511	0.00405
ℓ_O	∞	0.0700	0.0318	0.0167	0.00161	∞	0.00791	0.00243	0.00185	0.00234
L_B	∞	0.424	0.264	0.195	0.103	∞	0.390	0.207	0.151	0.0896

field $\theta(\mathbf{x}, t) = (\gamma/N)(\rho - \overline{\rho})$ read

$$\partial_t \mathbf{u} + \mathbf{u} \cdot \boldsymbol{\nabla} \mathbf{u} = -\boldsymbol{\nabla} p - f \mathbf{e}_z \times \mathbf{u} \qquad (1)$$
$$- N \theta \mathbf{e}_z + \nu \nabla^2 \mathbf{u} + \boldsymbol{\Phi},$$
$$\partial_t \theta + \mathbf{u} \cdot \boldsymbol{\nabla} \theta = N w + \kappa \nabla^2 \theta, \qquad (2)$$

where $p(\mathbf{x}, t)$ denotes the reduced pressure, ν the kinematic viscosity and κ thermal diffusivity. Here, we choose $\nu = \kappa$, or equivalently, $\mathrm{Pr} = \nu/\kappa = 1$. Equations (2), (1) are integrated in a triply periodic box of resolution $M = 512, 1024$ by means of the pseudo-spectral solver GHOST (Geophysical High-Order Suite for Turbulence) [35] with a 2-nd order explicit Runge-Kutta scheme for the time stepping. To sustain turbulence and to achieve a statistically stationary state, an external mechanical isotropic forcing $\boldsymbol{\Phi}(\mathbf{x}, t)$ is included to inject energy at large scale in a narrow wave number band within the range $2 \leq k_\Phi \leq 3$, hence the resulting characteristic forcing length scale $L_\Phi = 2\pi/2.5$. The rate of kinetic energy injection reads $\varepsilon_\Phi = \langle \mathbf{u} \cdot \boldsymbol{\Phi} \rangle$. To quantify the relative strength of turbulence, stratification and rotation, we consider the dimensionless Reynolds (Re), Froude (Fr) and Rossby (Ro) numbers at forcing scale L_Φ, given by

$$\mathrm{Re} = \frac{u' L_\Phi}{\nu}, \quad \mathrm{Fr} = \frac{u'}{L_\Phi N}, \quad \mathrm{Ro} = \frac{u'}{L_\Phi f}, \qquad (3)$$

where u', defined as the root mean square of the velocity fluctuation $u' = \langle |\mathbf{u}|^2 \rangle^{1/2}$, is the characteristic velocity of the large-scale flow. The ratio $N/f = \mathrm{Ro}/\mathrm{Fr}$ measures the relative strength of stratification and rotation. In the present simulations, we chose to fix $N/f = 5$, which is found in the Southern Ocean [26, 27]. The typical vertical length scale of stratification layers is given by the buoyancy scale [31, 33]

$$L_B = u'/N. \qquad (4)$$

To compare the relative strength of stratification and dissipation on small scales, i.e. the relative importance of internal-gravity waves and vortices, we define the buoyancy Reynolds number $R_{\mathrm{IB}} = \varepsilon_\nu/(\nu N^2)$ [2], which is related to the ratio between the Ozmidov scale $\ell_O = (\varepsilon_\nu/N^3)^{1/2}$ and the Kolmogorov scale $\eta = (\nu^3/\varepsilon_\nu)^{1/4}$ as $R_{\mathrm{IB}} = (\ell_O/\eta)^{4/3}$. The former is the length scale below which stratification effects become negligible and the flow recovers isotropy, while the latter is the characteristic scale for dissipation. Alternatively, R_{IB} can be interpreted as a ratio between times as $R_{\mathrm{IB}} = (\tau_\eta N)^{-2}$, namely the viscous time $\tau_\eta = (\nu/\varepsilon_\nu)^{1/2}$ and the typical time of the internal gravity waves $\sim 1/N$. For the dynamics of single tracer particles, at transition between a wave-dominated ($R_{\mathrm{IB}} < 0$) and an eddy-dominated regime ($R_{\mathrm{IB}} > 0$) was recently observed [36]. The buoyancy Reynolds number R_{IB} used here is related to, but differs from $R_{\mathcal{B}} = \mathrm{Re Fr}^2$, see [37].

To ensure that our simulations are satisfactorily resolved, we kept $k_{\max}\eta \gtrsim 2$, where $k_{\max} = M/3$ is the largest wavenumber in the simulation. We choose a time increment $\mathrm{d}t$ sufficiently small so that the fastest waves are well resolved. The simulation parameters are summarized in table I.

While solving the Boussinesq equations (eqs. (1), (2)), we follow the trajectories of $N_p \gtrsim 10^6$ tracer particles, initially randomly distributed throughout the system. To obtain information of particle pairs from trajectories both forwards and backwards in time, we identify, at specific times, pairs of particles whose relative distance is within a chosen range of distance $r - \Delta r \leq |\mathbf{r}| \leq r + \Delta r$ with the tolerance Δr. For large databases, the computation time to compute all relative distances grows rapidly. For an efficient parallelized approach to this challenge we refer to [38]. Here, we focus on single processor optimization by employing a novel algorithm using hierarchical spatial domain partitioning with an octree data structure [39]. In test runs with synthetic data, we observed a reduction of computational time by a factor of up to
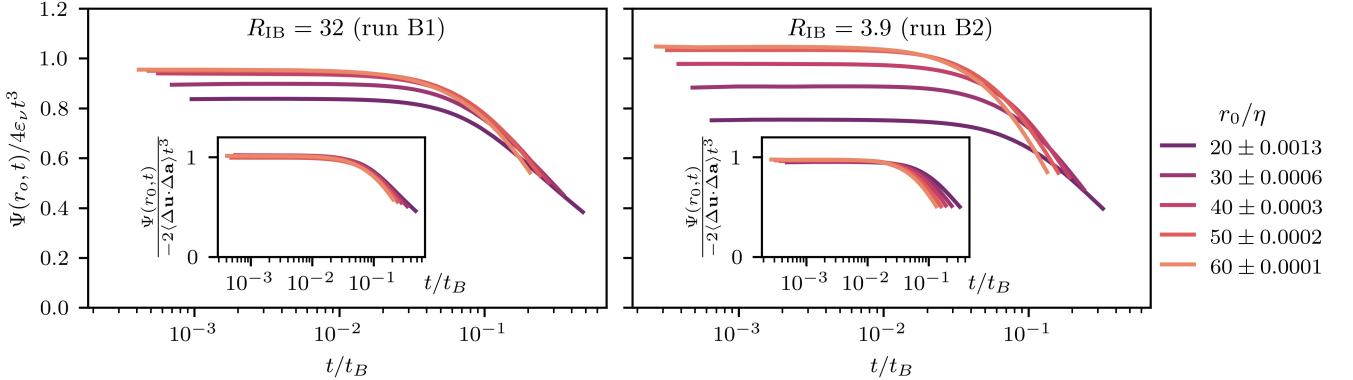
FIG. 1. Time anti-symmetric part of relative pair dispersion for different initial separations r_0 within the inertial range (indicated by color), compensated by the HIT prediction using $\langle \Delta_{r_0}\mathbf{u} \cdot \Delta_{r_0}\mathbf{a}\rangle = -2\varepsilon_\nu$. Compare with the previously studied HIT case [12]. The left panel shows run B1, with only small differences to the HIT case [12], the right panel shows, run B2 in table I showing a scale dependency of the pair dispersion time asymmetry. The inlets demonstrate the validity of the Taylor expansion in eq. (5) for both cases. Here, we used a different set of pairs to estimate $\Psi(r_0, t)$ and $\langle \Delta_{r_0}\mathbf{u} \cdot \Delta_{r_0}\mathbf{a}\rangle$ to avoid biasing the analysis.

10^3, depending on various parameters such as N_p, r and Δr. For a short description of the algorithm we refer to the supplemental material [40], for more details see [41]. For the analysis presented in the following, we chose the tolerances $\Delta r_0 \propto r_0^{-2}$ to keep the number of pairs independent of r_0. As a reference, we chose $\Delta r_0 = 0.005\eta$ for $r_0 = 10\eta$. We averaged over $\sim 10^6$ pairs per run and distance r_0 that are taken, assuming a statistically stationary flow, from 256 snapshots of the simulation.

A measure of the relative dispersion of two particles is provided by the evolution of the squared separation $\delta_{r_0}r(t)^2 = (\mathbf{r}(t) - \mathbf{r}_0)^2$, imposing that the initial separation $\mathbf{r}(0) = \mathbf{r}_0$ [12, 42–45]. Focusing on short times, a straightforward Taylor series expansion leads to:

$$\delta_{r_0}r(t)^2 \approx (\Delta_{r_0}\mathbf{u})^2 t^2 + (\Delta_{r_0}\mathbf{u} \cdot \Delta_{r_0}\mathbf{a})t^3, \quad (5)$$

where $\Delta_{r_0}\mathbf{u}$ and $\Delta_{r_0}\mathbf{a}$ denote the initial value of the pairs relative velocity and acceleration respectively [42]. Note that eq. (5) holds for the motion of particle pairs in any Newtonian system. By averaging over all pairs of particles with the same initial separation, the cubic term in eq. (5) provides a direct connection with the intrinsic time-asymmetry of the flow, as it was the case for HIT [12]. Inserting eq. (5) we obtain, for the function Ψ characterizing the asymmetry of $\delta_{r_0}r(t)^2$:

$$\Psi(r_0, t) \equiv \langle \delta_{r_0}r^2(-t) - \delta_{r_0}r^2(t)\rangle \approx -2\langle \Delta_{r_0}\mathbf{u} \cdot \Delta_{r_0}\mathbf{a}\rangle t^3. \quad (6)$$

The approximate expression eq. (5) is estimated to remain valid over the Bachelor time $t_B(r_0) = \left|\langle(\Delta_{r_0}\mathbf{u})^2\rangle / \langle\Delta_{r_0}\mathbf{u} \cdot \Delta_{r_0}\mathbf{a}\rangle\right|$ [42, 46]. For HIT, assuming $\langle(\Delta_{r_0}\mathbf{u})^2\rangle \propto \varepsilon_\nu^{2/3} r_0^{2/3}$ and $\langle\Delta_{r_0}\mathbf{u} \cdot \Delta_{r_0}\mathbf{a}\rangle = -2\varepsilon_\nu$, t_B reduces to the Kolmogorov time: $t_B(r_0) \propto \varepsilon_\nu^{-1/3} r^{2/3} = \tau_{r_0}$. For ROTSTRAT turbulence, $\langle(\Delta_{r_0}\mathbf{u})^2\rangle$ follows a different scaling law with r_0 [2, 24]. Here, we merely determine

t_B as the ratio between $\langle(\Delta_{r_0}\mathbf{u})^2\rangle$ and $\langle\Delta_{r_0}\mathbf{u} \cdot \Delta_{r_0}\mathbf{a}\rangle$, measured from our own simulations.

Figure 1 shows that contrary to the HIT case, where $\Psi(r_0, t)/t^3 \approx 4\varepsilon_\nu$ is independent of r_0, provided that r_0 is in the inertial range and $t \ll t_B$ [12], in the ROTSTRAT case, $\Psi(r_0, t)/t^3$ is a function of r_0, which increases with the initial separation r_0, the more so as Fr decreases.

In eq. (6), we identify the average rate of change of the pairs kinetic energy $\langle \mathrm{D}/\mathrm{D}t\, E_{\mathrm{kin}}^{(r_0)}\rangle = \langle\Delta_{r_0}\mathbf{u} \cdot \Delta_{r_0}\mathbf{a}\rangle$. To proceed, we extend the one-particle energy budget to the pair energy budget. The former is obtained by averaging the Boussinesq equations (eqs. (1), (2)). Assuming homogeneity and stationarity, one finds (see [40]):

$$\varepsilon_\Phi - \varepsilon_\nu - N\langle\theta w\rangle = 0 \quad \text{and} \quad N\langle\theta w\rangle - \varepsilon_\kappa = 0, \quad (7)$$

where ε_Φ is the energy source, and ε_ν and ε_κ are respectively the dissipation terms for the kinetic and potential energy. The exchange term $N\langle\theta w\rangle$ represents the amount of kinetic energy converted into potential energy. This term is positive and equal to the amount of dissipated potential energy ε_κ [25]. The Lagrangian two-point energy budget, describing the transfer of energy between two particles, generalizes the classical Karman-Howarth-Monin relations. By averaging over the Boussinesq equations (eqs. (1), (2)), assuming homogeneity and stationarity [9, 25, 47], we obtain (see [40]):

$$\langle\Delta_{r_0}\mathbf{u} \cdot \Delta_{r_0}\mathbf{a}\rangle = -2\varepsilon_\nu - N\langle\Delta_{r_0}\theta\Delta_{r_0}w\rangle - 2D_\nu(r_0), \quad (8)$$

$$\left\langle\Delta_{r_0}\theta \cdot \Delta_{r_0}\dot\theta\right\rangle = -2\varepsilon_\kappa + N\langle\Delta_{r_0}\theta\Delta_{r_0}w\rangle - 2D_\kappa(r_0), \quad (9)$$

with the mixed dissipation terms $D_\nu(r_0) = \nu\left\langle\sum_{i,j} \frac{\partial u_i(\mathbf{x})}{\partial x_j}\frac{\partial u_i(\mathbf{x+r})}{\partial x_j}\right\rangle$ and $D_\kappa(r_0) = \kappa\left\langle\sum_j \frac{\partial\theta(\mathbf{x})}{\partial x_j}\frac{\partial\theta(\mathbf{x+r})}{\partial x_j}\right\rangle$. We assume the gradients to decorrelate quickly for sufficiently large separations r_0,
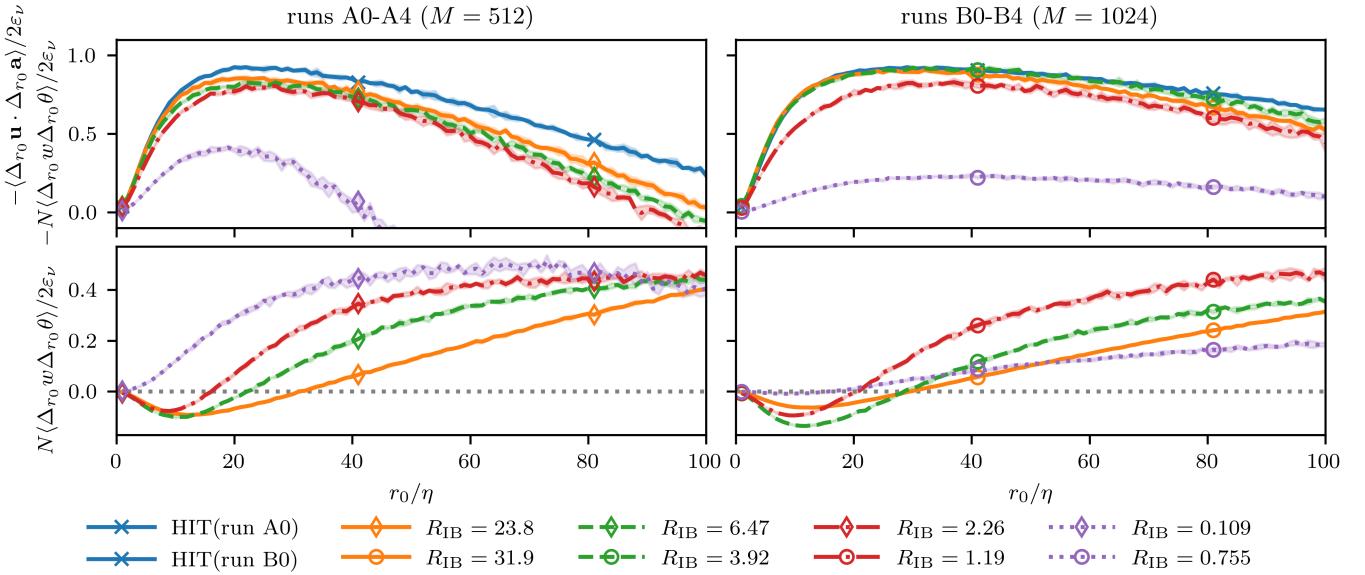
FIG. 2. Kinetic energy budget (first row) and exchange term (second row) for all runs. The left column shows the observations for the $M = 512$ runs (A0-A4) (diamonds), the right column those for the $M = 1024$ runs (B0-B4) (circles). Colors indicate different values of R_{IB}, as indicated in the legend. The shaded areas indicate the standard deviation computed averaging over 4 subsets. The lines correspond to the average over the whole data set. Furthermore, the dotted gray line in the second row denotes a vanishing energy exchange, i.e. $N\langle \Delta_{r_0}\theta\Delta_{r_0}w\rangle = 0$.

such that the mixed dissipation terms can be neglected. In the absence of stratification, the Karman-Howarth-Monin relation reduces to the well-known relation $\langle \Delta_{r_0}\mathbf{u}\cdot\Delta_{r_0}\mathbf{a}\rangle = -2\varepsilon_\nu$., valid in HIT. Furthermore, we note that all rotational terms vanish.

The signs of the various terms in eqs. (8), (9) determine the direction of the transfer. The negative sign of $-2\varepsilon_\nu$ is the signature of the presence of a direct energy cascade. We remark that in two-dimensional turbulence, the sign of the cross-correlation between acceleration and velocity is inverted. This is a consequence of the correlation between velocity and dissipation at large scales, whereas forcing acts at a much smaller scale, from which energy flux arranges in an inverse cascade [48, 49].

In our simulations, we observe the sum $-[\langle\Delta_{r_0}\mathbf{u}\cdot\Delta_{r_0}\mathbf{a}\rangle + N\langle\Delta_{r_0}w\Delta_{r_0}\theta\rangle]/2\varepsilon_\nu$ to be constant and close to unity over a certain range of scales (which increases with the Re) for runs with $R_{\mathrm{IB}} > 1$, as shown in the first row of fig. 2. According to eq. (8), this term is equal to $1 + D_\nu(r_0)/(2\varepsilon_\nu)$ and can thus be seen as the full kinetic energy budget. For the cases considered here with $R_{\mathrm{IB}} < 1$, we observe a stronger deviation from 1, possibly pointing to a transition to a different energy transfer mechanism.

Judging from eqs. (8), (9), the term $N\langle\Delta_{r_0}\theta\Delta_{r_0}w\rangle$, represents an average exchange from kinetic to potential energy if positive, or conversely if negative. In our simulations, we observe for large separations in the inertial range the average energy exchange to be positive, i.e. converting kinetic energy to potential energy. For small

separations and $R_{\mathrm{IB}} > 1$, however, we observe a negative average energy exchange, hence transferring energy in the opposite direction, i.e. from potential to kinetic energy, as shown in the second row of fig. 2. This result is consistent with other observations from Eulerian studies in spectral space [28–32].

We now consider the transition length scale ℓ_t, where the change of sign occurs, i.e. $N\langle\Delta_{\ell_t}\theta\Delta_{\ell_t}w\rangle = 0$. Figure 3 shows the ratio between ℓ_t and the buoyancy length-scale L_B as a function of R_{IB}. Although the ratio ℓ_t/L_B is not strictly constant, it remains of order 1 throughout the simulations with $R_{\mathrm{IB}} > 1$, where $0.035 \lesssim \mathrm{Fr} \lesssim 0.17$. This suggests that the mechanism leading to the energy exchange results from the complex interactions between internal gravity waves and turbulent eddies. The connection even prevails very close to the transition at $R_{\mathrm{IB}} = 1$ (see run B3 and B4). At even lower R_{IB}, we see a transition to a different regime. Furthermore, at the largest value of R_{IB} studied here, ℓ_t/L_B deviates more from ~ 1 than for the runs at lower values of R_{IB}. In addition, we remark that run B1 (full, yellow line with circles in fig. 2) shows a reduced exchange term at small scales compared to the other runs. This may indicate a different behavior, due to the large value of R_{IB}.

The observed energy exchange directly influences the time asymmetry in particle dispersion $\Psi(r_0, t)$, and explains the differences to the previously studied case of HIT [12]. For separations $r_0 > L_B$, the average energy transfer is directed from kinetic to potential energy and increases with r_0. This explains the observed increase
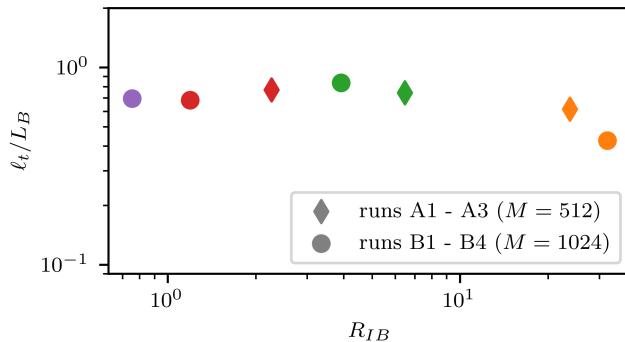
FIG. 3. Length scale ℓ_t at which the exchange term changes compensated by the buoyancy length scale L_B as a function of R_{IB}

of $\Psi(r_0, t)$ with increasing r_0 in fig. 1. For separations $\eta < r_0 < L_B$, the energy transfer is from potential to kinetic energy, symmetrically increasing and decreasing pair dispersion backwards and forwards in time and are therefore reducing the pair asymmetry $\Psi(r_0, t)$.

A precise description of the energy exchanges in rotating stratified turbulent flows is crucial to understand the interplay between waves and eddies. Remarkably, our work stresses the role of the buoyancy length scale, L_B, over a broad range of R_{IB} from an eddy dominated regime ($R_{\mathrm{IB}} \gtrsim 10$) [15] until the transitional regime to wave-dominated flows ($R_{\mathrm{IB}} \lesssim 1$). Interesting questions for future investigation are whether our conclusions extend to the range $100 \lesssim R_{\mathrm{IB}} \lesssim 1000$, corresponding to measurements in the oceans [50] and to similar values of R_{IB} at higher Re and lower Fr. We conclude by noticing that the time-asymmetry of the relative energy between two tracer particles could be used to measure the energy dissipation rate, ε_ν, in terrestrial or planetary flows [51, 52]. In this context, understanding of the exchange between kinetic and potential energy in such flows appears as an important step.

[1] J. Pedlosky, *Geophysical Fluid Dechanics* (Springer Verlag, New York, 1092).

[2] P. A. Davidson, *Turbulence in Rotating, Stratified and Electrically Conducting Fluids* (Cambridge University Press, Cambridge, 2013).

[3] S. A. Thorpe, *An Introduction to Ocean Turbulence* (Cambridge University Press, Cambridge, 2007).

[4] M. S. Miesch, Large-Scale Dynamics of the Convection Zone and Tachocline, Living Reviews in Solar Physics **2**, 1 (2005).

[5] A. S. Monin and A. M. Yaglom, *Statistical Fluid Mechanics, Volume II: Mechanics of Turbulence*, Vol. 2 (Courier Corporation, 2013).

[6] U. Frisch, *Turbulence: The Legacy of A. N. Kolmogorov* (Cambridge University Press, 1995).

[7] G. I. Taylor, Statistical theory of turbulenc, Proceedings of the Royal Society of London. Series A - Mathematical and Physical Sciences **151**, 421 (1935).

[8] A. Kolmogorov, The Local Structure of Turbulence in Incompressible Viscous Fluid for Very Large Reynolds' Numbers, Akademiia Nauk SSSR Doklady **30**, 301 (1941).

[9] J. Mann, S. Ott, and J. S. Andersen, *Experimental Study of Relative, Turbulent Diffusion*, Report 87-550-2370-3 (Risø National Laboratory, Roskilde, Denmark, 1999).

[10] G. Falkovich, K. Gawędzki, and M. Vergassola, Particles and fields in fluid turbulence, Reviews of Modern Physics **73**, 913 (2001).

[11] A. Pumir, B. I. Shraiman, and M. Chertkov, The Lagrangian view of energy transfer in turbulent flow, Europhysics Letters **56**, 379 (2001).

[12] J. Jucha, H. Xu, A. Pumir, and E. Bodenschatz, Time-reversal-symmetry Breaking in Turbulence, Physical Review Letters **113**, 054501 (2014).

[13] A. Cheminet, D. Geneste, A. Barlet, Y. Ostovan, T. Chaabo, V. Valori, P. Debue, C. Cuvier, F. Daviaud, J.-M. Foucaut, J.-P. Laval, V. Padilla, C. Wiertel-Gasquet, and B. Dubrulle, Eulerian vs Lagrangian Irreversibility in an Experimental Turbulent Swirling Flow, Physical Review Letters **129**, 124501 (2022).

[14] H. Xu, A. Pumir, G. Falkovich, E. Bodenschatz, M. Shats, H. Xia, N. Francois, and G. Boffetta, Flight–crash events in turbulence, Proceedings of the National Academy of Sciences **111**, 7558 (2014).

[15] A. Pouquet, D. Rosenberg, R. Marino, and C. Herbert, Scaling laws for mixing and dissipation in unforced rotating stratified turbulence, J. Fluid Mech. **844**, 519 (2018).

[16] C. Rorai, P. D. Mininni, and A. Pouquet, Turbulence comes in bursts in stably stratified flows, Physical Review E **89**, 043002 (2014).

[17] T. Dauxois, S. Joubaud, P. Odier, and A. Venaille, Instabilities of internal gravity wave beams, Annual review of fluid mechanics **50**, 131 (2018).

[18] F. Feraco, R. Marino, L. Primavera, A. Pumir, P. D. Mininni, D. Rosenberg, A. Pouquet, R. Foldes, E. Lévêque, E. Camporeale, S. S. Cerri, H. Charuvil Asokan, J. L. Chau, J. P. Bertoglio, P. Salizzoni, and M. Marro, Connecting large-scale velocity and temperature bursts with small-scale intermittency in stratified turbulence, EPL (Europhysics Letters) **135**, 14001 (2021).

[19] C. P. Caulfield, Layering, instabilities, and mixing in turbulent stratified flows, Annual Review of Fluid Mechanics **53**, 113 (2021), https://doi.org/10.1146/annurev-fluid-042320-100458.

[20] R. Marino, F. Feraco, L. Primavera, A. Pumir, A. Pouquet, D. Rosenberg, and P. D. Mininni, Turbulence gener-

ation by large-scale extreme vertical drafts and the modulation of local energy dissipation in stably stratified geophysical flows, Physical Review Fluids **7**, 033801 (2022).

[21] J. R. Taylor and A. F. Thompson, Submesoscale dynamics in the upper ocean, Annual Review of Fluid Mechanics **55**, 103 (2023), https://doi.org/10.1146/annurev-fluid-031422-095147.

[22] R. Marino, P. D. Mininni, D. Rosenberg, and A. Pouquet, Inverse cascades in rotating stratified turbulence: Fast growth of large scales, EPL (Europhysics Letters) **102**, 44006 (2013).

[23] R. Marino, A. Pouquet, and D. Rosenberg, Resolving the paradox of oceanic large-scale balance and small-scale mixing, Phys. Rev. Lett. **114**, 114504 (2015).

[24] A. Alexakis and L. Biferale, Cascades and transitions in turbulent flows, Physics Reports Cascades and Transitions in Turbulent Flows, **767−769**, 1 (2018).

[25] A. Sozza, G. Boffetta, P. Muratore-Ginanneschi, and S. Musacchio, Dimensional transition of energy cascades in stably stratified forced thin fluid layers, Physics of Fluids **27**, 035112 (2015).

[26] A. C. Naveira Garabato, K. L. Polzin, B. A. King, K. J. Heywood, and M. Visbeck, Widespread Intense Turbulent Mixing in the Southern Ocean, Science **303**, 210 (2004).

[27] M. Nikurashin, G. K. Vallis, and A. Adcroft, Routes to energy dissipation for geostrophic flows in the Southern Ocean, Nature Geoscience **6**, 48 (2013).

[28] G. Holloway, The buoyancy flux from internal gravity wave breaking, Dynamics of Atmospheres and Oceans **12**, 107 (1988).

[29] C. Staquet and F. S. Godeferd, Statistical modelling and direct numerical simulations of decaying stably stratified turbulence. Part 1. Flow energetics, Journal of Fluid Mechanics **360**, 295 (1998).

[30] G. F. Carnevale, M. Briscolini, and P. Orlandi, Buoyancy- to inertial-range transition in forced stratified turbulence, Journal of Fluid Mechanics **427**, 205 (2001).

[31] G. Brethouwer, P. Billant, E. Lindborg, and J.-M. Chomaz, Scaling analysis and simulation of strongly stratified turbulent flows, Journal of Fluid Mechanics **585**, 343 (2007).

[32] C. Rorai, P. D. Mininni, and A. Pouquet, Stably stratified turbulence in the presence of large-scale forcing, Physical Review E **92**, 013003 (2015).

[33] P. Billant and J.-M. Chomaz, Self-similarity of strongly stratified inviscid flows, Physics of Fluids **13**, 1645 (2001).

[34] M. L. Waite, Stratified turbulence at the buoyancy scale, Physics of Fluids **23**, 066602 (2011).

[35] P. D. Mininni, D. Rosenberg, R. Reddy, and A. Pouquet, A hybrid MPI–OpenMP scheme for scalable parallel pseudospectral computations for fluid turbulence, Parallel Computing **37**, 316 (2011).

[36] D. Buaria, A. Pumir, F. Feraco, R. Marino, A. Pouquet, D. Rosenberg, and L. Primavera, Single-particle Lagrangian statistics from direct numerical simulations of rotating-stratified turbulence, Physical Review Fluids **5**, 064801 (2020).

[37] G. N. Ivey, K. B. Winters, and J. R. Koseff, Density Stratification, Turbulence, but How Much Mixing?, Annual Review of Fluid Mechanics **40**, 169 (2008).

[38] D. Buaria, B. L. Sawford, and P. K. Yeung, Characteristics of backward and forward two-particle relative dispersion in turbulence at different Reynolds numbers, Physics of Fluids **27**, 105101 (2015).

[39] R. A. Finkel and J. L. Bentley, Quad trees a data structure for retrieval on composite keys, Acta Informatica **4**, 1 (1974).

[40] Supplemental material.

[41] S. Gallon, Ph.D. thesis (In preparation).

[42] G. K. Batchelor, The application of the similarity theory of turbulence to atmospheric diffusion, Quarterly Journal of the Royal Meteorological Society **76**, 133 (1950).

[43] M. Bourgoin, N. T. Ouellette, H. Xu, J. Berg, and E. Bodenschatz, The Role of Pair Dispersion in Turbulent Flow, Science **311**, 835 (2006).

[44] N. T. Ouellette, H. Xu, M. Bourgoin, and E. Bodenschatz, An experimental study of turbulent relative dispersion models, New Journal of Physics **8**, 109 (2006).

[45] J. I. Polanco, S. Arun, and A. Naso, Multiparticle Lagrangian statistics in homogeneous rotating turbulence, Physical Review Fluids **8**, 034602 (2023).

[46] R. Bitane, H. Homann, and J. Bec, Time scales of turbulent relative dispersion, Physical Review E **86**, 045302(R) (2012).

[47] R. J. Hill, Exact second-order structure-function relationships, Journal of Fluid Mechanics **468**, 317 (2002).

[48] D. Bernard, Three-point velocity correlation functions in two-dimensional forced turbulence, Physical Review E **60**, 6184 (1999).

[49] A. D. Bragg, F. De Lillo, and G. Boffetta, Irreversibility inversions in two-dimensional turbulence, Physical Review Fluids **3**, 024302 (2018).

[50] J. N. Moum, Energy-containing scales of turbulence in the ocean thermocline, J. Geophys. Res **101**, 14095 (1996).

[51] B. C. Pearson, J. L. Pearson, and B. Fox-Kemper, Advective structure functions in anisotropic two-dimensional turbulence, Journal of Fluid Mechanics **916**, A49 (2021).

[52] B. Pearson, C. Wagner, J. Pearson, N. Rodriguez, S. Alshenaiber, and B. Fox-Kemper, A new method to diagnose turbulent cascade rates in mesoscale ocean systems and planetary atmospheres (2023).

[53] L. D. Landau and E. M. Lifshitz, *Fluid Mechanics*, 2nd ed., Course of Theoretical Physics, Vol. 6 (Butterworth-Heinemann, Amsterdam Heidelberg, 1987).

Supplemental Material for:
Lagrangian irreversibility and energy exchanges in rotating-stratified turbulent flows

S. Gallon,[1] A. Sozza,[1,2] F. Feraco,[3,4] R. Marino,[3] and A. Pumir[1,5]

[1] *Univ Lyon, ENS de Lyon, CNRS, Laboratoire de Physique, F-69342 Lyon, France*
[2] *CNR, Institute of Atmospheric Sciences and Climate, 10133 Torino, Italy*
[3] *Univ Lyon, CNRS, École Centrale de Lyon, INSA de Lyon, Univ Claude Bernard Lyon 1,*
Laboratoire de Mécanique des Fluides et d'Acoustique - UMR 5509, F-69134 Écully, France
[4] *Leibniz-Institute of Atmospheric Physics at the Rostock University, 18225 Kühlungsborn, Germany*
[5] *Max Planck Institute for Dynamics and Self-Organization, 37077 Göttingen, Germany*
(Dated: January 25, 2024)

OCTREE BASED ALGORITHM FOR PARTICLE PAIR IDENTIFICATION

Experimental and numerical studies of turbulent flows often generate very large databases. The present investigation in Lagrangian turbulence relies on the analysis of millions of particle trajectories. Extracting meaningful information on the structure of the flow, as a function of scale r, rests on the capability to identify sets of particles separated by a distance r, up to a tolerance Δr. The corresponding search through the database, however, can be a very expensive task, the more so as the total number of particles N_p, increases. This calls for the development of efficient methods to search through the database.

A way to reduce computational costs is to divide the domain into sub-domains, e.g. into sub-cubes of edge length ℓ and sort all the particles into these sub-cubes. When $r + \Delta r < \ell$, the particles within a distance between $r - \Delta r$ and $r + \Delta r$ from a given particle p_1 are either in the same sub-cube as p_1 or in one of the neighboring 26 sub-cubes. Restricting the search to these sub-cubes can lead to a significant reduction of the computational effort. To further improve the performance especially for larger separations r between particles, we propose a search algorithm based on the octree data structure [1]. Within this approach, the original cubic domain, $[0, 2\pi]^3$, is subdivided into 8 sub-cubes with each half the original side length. The original cube is referred to as the root node and the sub-cubes as its children. Each of the children nodes is then itself recursively subdivided into 8 sub-cubes per generation, with each half the side length of the previous generation. The process is repeated for a total of m times. The particles are then sorted into the 8^m smallest sub-cubes (leaf nodes). For the present application, we assume the particles to be uniformly distributed (note that for some other applications of the octree-data structure, the number of refinements is chosen locally based on the local particle density). To choose the number of refinements m, we found that the method works efficiently with at least ~ 10 particles per cube on the smallest level.

Particles at a separation within $[r - \Delta r, r + \Delta r]$ to a particle p_1 are located in a shell, as represented for the two-dimensional case in fig. 1(a). To find these particles, we start at the root node and descent in the tree to the child node that contains the position of p_1. We repeat this descent until we arrive at a node whose side length ℓ_i fulfills $\ell_i/2 < r + \Delta r < \ell_i$, which is the node with the smallest side length that is still larger than the maximum search distance $r + \Delta r$. All particles that are at distance $r \pm \Delta r$ to p_1 can therefore be only either within this node, or within one of its neighbors , see fig. 1(b). We then look for all the nodes of smaller size that intersect with the shell by the following recursive approach. A given node can contain a particle at a distance between $r - \Delta r$ and $r + \Delta r$ from a particle p_1 only if it has an intersection with the shell represented in fig. 1. Therefore, if a node is either too close or too far away from p_1, itself and its children can be discarded. The children of the nodes that have an intersection with the shell are considered in the next step, using the same procedure until the leaf nodes are reached (see fig. 1(c-f)). To finalize the search, we compute the distances of the particles in the remaining nodes to p_1 to find all pair partners. This procedure is repeated for all p_1 to find all possible pairs. To avoid double counting, we only keep pairs with increasing indices, i.e. $p_1 < p_2$.

DERIVATION OF THE PAIR ENERGY BUDGET

In this work, we consider a stably stratified fluid with a linear density profile $\overline{\rho} = \rho_0 - \gamma z$ in a rotating frame of reference with solid body rotation rate Ω (and frequency $f = 2\Omega$). In this case, the equations of motion for the
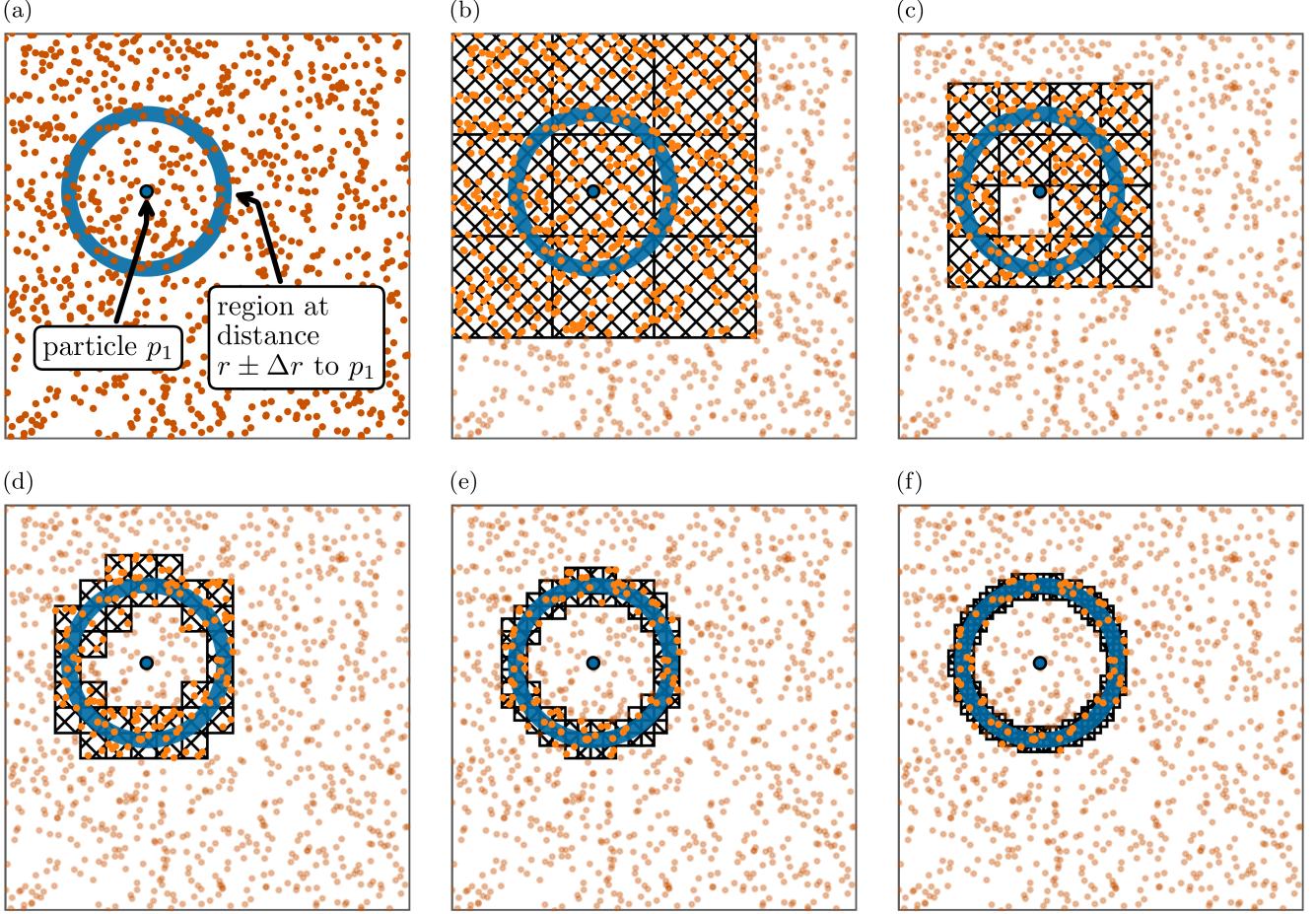
FIG. 1. Exemplary depiction of the pair search algorithm using a quadtree-data structure in two dimensions. (a-f) The blue point with black edge is the particle $p1$, the shell of distances $r \pm \Delta r$ is colored in blue. (b-f) Iterative search using the quadtree data structure. The hatched regions are the nodes that intersect with the shell in the respective generation.

incompressible velocity field $\mathbf{u} = (u, v, w)$, i.e. $\boldsymbol{\nabla} \cdot \mathbf{u} = 0$ and density fluctuation $\theta = (\gamma/N)(\rho - \overline{\rho})$ read

$$\partial_t \mathbf{u} + \mathbf{u} \cdot \boldsymbol{\nabla} \mathbf{u} = -\boldsymbol{\nabla} p - f\mathbf{e}_z \times \mathbf{u} - N\theta\mathbf{e}_z + \nu\nabla^2\mathbf{u} + \boldsymbol{\Phi}, \tag{1}$$

$$\partial_t \theta + \mathbf{u} \cdot \boldsymbol{\nabla} \theta = Nw + \kappa\nabla^2\theta, \tag{2}$$

with the reduced pressure p, the Brunt-Väisälä frequency $N = (\gamma g/\rho_0)^{1/2}$, the kinematic viscosity ν, the external forcing Φ and the thermal diffusivity κ.

In the following, we derive the energy budget for the relative kinetic and potential energy for two particles separated by $\mathbf{r}$. For the original Eulerian work, we refer to [2].

One Particle Energy Budget

We start by considering a single particle with velocity $\mathbf{u}$ and acceleration $\mathbf{a} = \frac{\mathrm{D}}{\mathrm{D}t}\mathbf{u} = \partial_t\mathbf{u} + \mathbf{u} \cdot \boldsymbol{\nabla}\mathbf{u}$. The rate of change of the kinetic energy $E_{\mathrm{kin}} = \mathbf{u}^2/2$ of this particle along its trajectory is given by

$$\frac{\mathrm{D}}{\mathrm{D}t}E_{\mathrm{kin}} = \mathbf{u} \cdot \mathbf{a}. \tag{3}$$

Averaging this quantity over many particles and inserting the equation of motion, we obtain

$$\left\langle \frac{\mathrm{D}}{\mathrm{D}t}E_{\mathrm{kin}} \right\rangle = -\langle \mathbf{u} \cdot \boldsymbol{\nabla} p \rangle - \langle \mathbf{u} \cdot f\mathbf{e}_z \times \mathbf{u} \rangle - \langle \mathbf{u} \cdot N\theta\mathbf{e}_z \rangle + \langle \mathbf{u} \cdot \nu\nabla^2\mathbf{u} \rangle + \langle \mathbf{u} \cdot \boldsymbol{\Phi} \rangle. \tag{4}$$

The first term on the right hand side of eq. (4) can be rewritten as

$$\langle \mathbf{u} \cdot \boldsymbol{\nabla} p \rangle = \boldsymbol{\nabla} \cdot \langle \mathbf{u} \cdot p \rangle - \langle p \boldsymbol{\nabla} \cdot \mathbf{u} \rangle = 0, \tag{5}$$

and therefore vanishes due to homogeneity (first term) and incompressibility (second term).

The second term on the right hand side of eq. (4) is zero for geometric reasons ($\mathbf{u} \cdot \mathbf{e}_z \times \mathbf{u} = 0$).

The third term on the right hand side of eq. (4) represents the energy exchange between potential and kinetic energy. For a more compact notation, we introduce

$$\varepsilon_\chi \equiv \langle \mathbf{u} \cdot N\theta \mathbf{e}_z \rangle = N \langle w\theta \rangle, \tag{6}$$

where w denotes the vertical velocity component. With our sign conventions, ε_χ represents a sink of kinetic energy and a source of potential energy for $\varepsilon_\chi > 0$.

The fourth term on the right hand side of eq. (4) describes the energy dissipation by viscosity

$$\left\langle \mathbf{u} \cdot \nu \nabla^2 \mathbf{u} \right\rangle = \frac{\nu}{2} \nabla^2 \left\langle (\mathbf{u})^2 \right\rangle - \varepsilon_\nu. \tag{7}$$

The first term on the right hand side of the equation above vanishes due to homogeneity. Furthermore we introduced the kinetic energy dissipation rate

$$\varepsilon_\nu \equiv \nu \left\langle \sum_{i,j} \left(\frac{\partial u_i}{\partial x_j} \right)^2 \right\rangle. \tag{8}$$

Finally, the remaining term on the right hand side of eq. (4) is the insertion of energy due to the large scale forcing $\boldsymbol{\Phi}$. For a more compact notation, we introduce

$$\varepsilon_\Phi \equiv \langle \mathbf{u} \cdot \boldsymbol{\Phi} \rangle. \tag{9}$$

Putting everything together, we arrive at the one point budget for the kinetic energy

$$\left\langle \frac{\mathrm{D}}{\mathrm{D}t} E_{\mathrm{kin}} \right\rangle = \langle \mathbf{u} \cdot \mathbf{a} \rangle = \varepsilon_\Phi - \varepsilon_\chi - \varepsilon_\nu. \tag{10}$$

For the potential energy $E_{\mathrm{pot}} = \theta^2/2$, we rewrite the thermal diffusive term similarly to the viscous term and directly obtain similarly the budget

$$\left\langle \frac{\mathrm{D}}{\mathrm{D}t} E_{\mathrm{pot}} \right\rangle = \langle \theta \dot{\theta} \rangle = \varepsilon_\chi - \varepsilon_\kappa, \tag{11}$$

with the potential energy dissipation rate

$$\varepsilon_\kappa \equiv \kappa \left\langle \sum_j \left(\frac{\partial \theta}{\partial x_j} \right)^2 \right\rangle. \tag{12}$$

Two Particle Energy Budget

We now consider a pair of particles with positions $\mathbf{x}^{(1)}(t)$ and $\mathbf{x}^{(2)}(t)$, separated by a displacement $\mathbf{r}(t)$, where $|\mathbf{r}(0)| = r$ is in the inertial range, and study the evolution of the relative kinetic energy of this pair $E_{\mathrm{kin}}^{(\mathbf{r})} = \Delta_{\mathbf{r}} \mathbf{u}^2/2$:

$$\frac{\mathrm{D}}{\mathrm{D}t} E_{\mathrm{kin}}^{(2)} = \Delta_{\mathbf{r}} \mathbf{u} \cdot \Delta_{\mathbf{r}} \mathbf{a}, \tag{13}$$

where we have used the notation $\Delta_{\mathbf{r}} q \equiv q^{(2)} - q^{(1)}$ for any observable q. Averaging eq. (13) over many pairs with the *same* separation $\mathbf{r}$, and using the Boussinesq equations, one obtains:

$$\left\langle \frac{\mathrm{D}}{\mathrm{D}t} E_{\mathrm{kin}}^{(2)} \right\rangle_{\mathbf{r}} = \left\langle \mathbf{u}^{(2)} \cdot \mathbf{a}^{(2)} \right\rangle_{\mathbf{r}} - \left\langle \mathbf{u}^{(2)} \cdot \mathbf{a}^{(1)} \right\rangle_{\mathbf{r}} - \left\langle \mathbf{u}^{(1)} \cdot \mathbf{a}^{(2)} \right\rangle_{\mathbf{r}} + \left\langle \mathbf{u}^{(1)} \cdot \mathbf{a}^{(1)} \right\rangle_{\mathbf{r}}. \tag{14}$$

Note that we are not only prescribing here the length of $\mathbf{r}$, but also its orientation. The first and last term on the right hand side of eq. (14) are the rates of change of the kinetic energy of each of the two particles separately. Because of statistical homogeneity, they are independent of the initial separation $\mathbf{r}$ and therefore each term is given by the single particle budget for the kinetic energy derived above:

$$\left\langle \mathbf{u}^{(2)} \cdot \mathbf{a}^{(2)} \right\rangle_{\mathbf{r}} = \left\langle \mathbf{u}^{(1)} \cdot \mathbf{a}^{(1)} \right\rangle_{\mathbf{r}} = \varepsilon_\Phi - \varepsilon_\chi - \varepsilon_\nu. \tag{15}$$

To evaluate the mixed terms on the right hand side of eq. (14), we first use arguments similar to those used for the one-particle energy budget to show that pressure terms do not contribute. As an example:

$$\left\langle \mathbf{u}^{(2)} \boldsymbol{\nabla}^{(1)} p^{(1)} \right\rangle_{\mathbf{r}} = \boldsymbol{\nabla}^{(1)} \cdot \left\langle \mathbf{u}^{(2)} p^{(1)} \right\rangle_{\mathbf{r}} - \left\langle p^{(2)} \boldsymbol{\nabla}^{(2)} \cdot \mathbf{u}^{(1)} \right\rangle_{\mathbf{r}} = 0, \tag{16}$$

where, we used $\boldsymbol{\nabla}^{(2)} \cdot \mathbf{u}^{(1)} = \boldsymbol{\nabla}^{(1)} \cdot \mathbf{u}^{(1)} = 0$.

The sum of the mixed terms involving the rotational (Coriolis force) vanishes as a consequence of the anti-symmetry of the cross product

$$\left\langle \mathbf{u}^{(2)} \cdot f\mathbf{e}_z \times \mathbf{u}^{(1)} \right\rangle_{\mathbf{r}} + \left\langle \mathbf{u}^{(1)} \cdot f\mathbf{e}_z \times \mathbf{u}^{(2)} \right\rangle = f\mathbf{e}_z \cdot \left\langle \mathbf{u}^{(2)} \times \mathbf{u}^{(1)} + \mathbf{u}^{(1)} \times \mathbf{u}^{(2)} \right\rangle = 0. \tag{17}$$

The mixed terms involving the density fluctuation θ cannot be eliminated. Together with the contribution from the single particle budgets of each of the particles, we obtain

$$2\varepsilon_\chi - \left\langle w^{(2)} N\theta^{(1)} \right\rangle_{\mathbf{r}} - \left\langle w^{(1)} N\theta^{(2)} \right\rangle_{\mathbf{r}} = N \left\langle \Delta_{\mathbf{r}} w \Delta_{\mathbf{r}} \theta \right\rangle_{\mathbf{r}}, \tag{18}$$

In this work, we consider a forcing on the large scales. We thus assume it to vary little for sufficiently small r and write $\boldsymbol{\Phi}^{(2)} \approx \boldsymbol{\Phi}^{(1)}$. The forcing contribution from the mixed particle terms thus read

$$-\langle \mathbf{u}^{(2)} \cdot \boldsymbol{\Phi}^{(1)} \rangle - \langle \mathbf{u}^{(1)} \cdot \boldsymbol{\Phi}^{(2)} \rangle \approx -2\varepsilon_\Phi \tag{19}$$

and cancel out the $+2\varepsilon_\Phi$ from the single particle terms.

To simplify the mixed viscous terms, we rewrite their sum

$$\left\langle \mathbf{u}^{(2)} \cdot \nu \left(\nabla^{(1)}\right)^2 \mathbf{u}^{(1)} \right\rangle_{\mathbf{r}} + \left\langle \mathbf{u}^{(1)} \cdot \nu \left(\nabla^{(2)}\right)^2 \mathbf{u}^{(2)} \right\rangle_{\mathbf{r}} = \nu \left(\nabla^{(1)}\right)^2 \left\langle \mathbf{u}^{(1)} \mathbf{u}^{(2)} \right\rangle_{\mathbf{r}} - 2D_\nu(\mathbf{r}), \tag{20}$$

where the first term on the right hand side vanishes due to homogeneity and with the mixed dissipation term

$$D_\nu(\mathbf{r}) \equiv \nu \left\langle \sum_{i,j} \left(\frac{\partial u_i^{(1)}}{\partial x_j^{(1)}}\right) \left(\frac{\partial u_i^{(2)}}{\partial x_j^{(2)}}\right) \right\rangle_{\mathbf{r}}. \tag{21}$$

Putting everything together, we obtain the two point budget for the kinetic pair energy

$$\left\langle \frac{\mathrm{D}}{\mathrm{D}t} E_{\mathrm{kin}}^{(2)} \right\rangle_{\mathbf{r}} = \langle \Delta_{\mathbf{r}} \mathbf{u} \cdot \Delta_{\mathbf{r}} \mathbf{a} \rangle_{\mathbf{r}} = -2\varepsilon_\nu - N \langle \Delta_{\mathbf{r}} w \Delta_{\mathbf{r}} \theta \rangle_{\mathbf{r}} - 2D_\nu(\mathbf{r}). \tag{22}$$

Similarly, we obtain the two particle budget for the potential pair energy $E_{\mathrm{pot}}^{(2)} = \theta^2/2$:

$$\left\langle \frac{\mathrm{D}}{\mathrm{D}t} E_{\mathrm{pot}}^{(2)} \right\rangle_{\mathbf{r}} = \left\langle \Delta_{\mathbf{r}} \theta \cdot \Delta_{\mathbf{r}} \dot{\theta} \right\rangle = -2\varepsilon_\kappa + N \langle \Delta_{\mathbf{r}} \theta \Delta_{\mathbf{r}} w \rangle - 2D_\kappa(\mathbf{r}). \tag{23}$$

with the mixed thermal diffusion term

$$D_\kappa(\mathbf{r}) \equiv \kappa \left\langle \sum_j \frac{\partial \theta^{(1)}}{\partial x_j} \frac{\partial \theta^{(2)}}{\partial x_j} \right\rangle_{\mathbf{r}}. \tag{24}$$

Comment on Isotropy

We note that in the derivation above, we did not explicitly assume the system to be isotropic. In fact, the flows we are considering here are largely anisotropic. In classical textbooks for the case of Navier-Stokes turbulence, the velocity-pressure gradient correlations are normally eliminated under the assumption of isotropy [3, 4]. It was then later demonstrated, that the derivation can alternatively be performed by assuming solely homogeneity and incompressibility [5–7]. Furthermore, we note that in the derivation of the pair energy budget, we explicitly fixed the orientation of the separation vector $\mathbf{r}$. The energy budgets are thus valid when averaging for any fixed distance and orientation, e.g. by prescribing the angle ϑ between the two particles and the z-axis, or when averaging over all orientations as we do in the present work.

Comment on Stationarity

In the derivation above, we did not explicitly assume stationarity. Equations (10), (11), (22) and (23) should thus also hold at any point in time in a non-stationary system, such as decaying turbulence. Note that then, quantities on both sides of the equations are time-depended.

In our simulations, we have considered statistically steady flows. For this reason, we expect that all quantities on the right hand side of eqs. (10), (11), (22) and (23) reach a statistical equilibrium. Assuming ergodicity, we compute the Lagrangian averages over particle positions and time, as pointed out in the main manuscript.

In a stationary state, the one particle energy budgets simplify to

$$\left\langle \frac{\mathrm{D}}{\mathrm{D}t} E_{\mathrm{kin}} \right\rangle = 0 = \langle \mathbf{u} \cdot \mathbf{a} \rangle = \varepsilon_\Phi - \varepsilon_\chi - \varepsilon_\nu, \tag{25}$$

$$\left\langle \frac{\mathrm{D}}{\mathrm{D}t} E_{\mathrm{pot}} \right\rangle = 0 = \langle \theta \dot{\theta} \rangle = \varepsilon_\chi - \varepsilon_\kappa. \tag{26}$$

Hence, velocity and acceleration are correlated in such a way that their scalar product on average is zero.

The left-hand side of the two-particle energy, using the Lagrangian point of view, remains non-zero, even when the flow is statistically steady, as the cross-correlation between velocity and acceleration is not vanishing. We stress that in this case, the identity

$$\langle \Delta_{\mathbf{r}} \mathbf{u} \cdot \Delta_{\mathbf{r}} \mathbf{a} \rangle_{\mathbf{r}} = \frac{1}{2} \nabla \cdot \left\langle |\Delta_{\mathbf{r}} \mathbf{u}|^2 \Delta_{\mathbf{r}} \mathbf{u} \right\rangle_{\mathbf{r}} \tag{27}$$

establishes a connection with the Karman-Howarth-Monin in the Eulerian framework [2].

[1] R. A. Finkel and J. L. Bentley, Quad trees a data structure for retrieval on composite keys, Acta Informatica **4**, 1 (1974).
[2] A. Sozza, G. Boffetta, P. Muratore-Ginanneschi, and S. Musacchio, Dimensional transition of energy cascades in stably stratified forced thin fluid layers, Physics of Fluids **27**, 035112 (2015).
[3] U. Frisch, *Turbulence: The Legacy of A. N. Kolmogorov* (Cambridge University Press, 1995).
[4] L. D. Landau and E. M. Lifshitz, *Fluid Mechanics*, 2nd ed., Course of Theoretical Physics, Vol. 6 (Butterworth-Heinemann, Amsterdam Heidelberg, 1987).
[5] J. Mann, S. Ott, and J. S. Andersen, *Experimental Study of Relative, Turbulent Diffusion*, Report 87-550-2370-3 (Risø National Laboratory, Roskilde, Denmark, 1999).
[6] R. J. Hill, Exact second-order structure-function relationships, Journal of Fluid Mechanics **468**, 317 (2002).
[7] R. J. Hill, Opportunities for use of exact statistical equations, Journal of Turbulence **7**, N43 (2006).